Composites: Part A 82 (2016) 235–242

Contents lists available at ScienceDirect

Composites: Part A

journal homepage: www.elsevier.com/locate/compositesa

Improved fatigue performance for wood-based structural panels using slot and tab construction

Jinghao Li [a,b], John F. Hunt [b,*], Shaoqin Gong [a], Zhiyong Cai [b,*]

[a] Department of Biomedical Engineering, Wisconsin Institutes for Discovery, and Materials Science and Engineering, University of Wisconsin-Madison, Madison, WI 53715, United States

[b] USDA Forest Service, Forest Products Laboratory, Madison, WI 53726, United States

ARTICLE INFO

Article history:
Received 11 September 2015
Received in revised form 21 December 2015
Accepted 27 December 2015
Available online 5 January 2016

Keywords:
A. Biocomposite
B. Fatigue
D. Mechanical testing
E. Joints/joining

ABSTRACT

This paper presents static and fatigue bending behavior for a wood-based structural panel having a slot and tab (S/T) construction technique. Comparisons were made with similarly fabricated panels without the S/T construction technique. Experimental results showed that both types of panels had similar bending properties in the static tests. However, the panels with S/T construction had better fatigue results. The failure modes were different for the two fabrication techniques. The panels without S/T debonded at the core:face interface. Whereas, the panels with S/T had cracks that propagated within the rib of the core after debonding damage at the core:face interface. The fatigue deflection-life relationship indicated that the S/T construction improved the connection between the faces and core. The S/T construction decreased the deflection growth rate that delayed panel failure. The fatigue stress-life relationship or degradation was better for the panels with S/T construction than the panels without the S/T construction.

1. Introduction

Structural composites have been widely used in many applications such as shipping, aerospace, transportation, and building construction due to its high strength-to-weight ratio [1–4]. Various materials, designs, and manufacturing, methods for structural composites attempting to improve performance have been developed and investigated in recent years. Isogrid core designs made from aluminum to fabricate structural composites for aerospace applications have shown that the isogrid configurations were more structurally efficiency than either foam or honeycomb structures [5,6]. The simple manufacturing process using interlocked grid structures with improved mechanical performance by unidirectional pultruded glass fiber rib was presented by Han and Tsai [7]. It was easier and more efficient than the traditional pultruded method. Fan et al. [8] fabricated interlocked kagome structural panels using carbon fiber composites and evaluated the mechanical behaviors using static compression and bending tests. The results indicated that debonding was one of the more significant failure modes for the mechanical tests. For fatigue tests, Belingardi et al. investigated the fatigue behavior of a sandwich beam using the four point bending test, two different failure mechanisms of face compression and core debonding were observed using both undamaged and initially damaged panels [9]. Jen et al. analyzed the effect of the amount of adhesive on the bending fatigue strength of bonded aluminum structural beams, the results showed the fatigue strength of structural beams was improved as the amount of adhesive increased [10]. Their research also demonstrated that the thickness of the face sheets showed no evidence of effect on the fatigue strength [11]. From the researches cited above, there was a common behavior observed that the core:face interface strength had a significant effect on the mechanical behavior of the structural composites, especially for fatigue.

Forest Products Laboratory (FPL) is working to develop engineered structural materials made from wood-fiber-based composites that have enhanced performance for some engineered applications such as air pallet, tactical shelter, transportation, or building construction materials [12–19]. In an initial study, phenolic laminated paper was used for a tri-axial core configuration within a structural composite panel. The mechanical behavior for these tri-axial core panels were obtained using static bending and compression tests [12–17]. The results showed these wood-based structural panels had good mechanical performance. However, debonding at the interface between the structural core and face caused premature failure during the mechanical tests. Failure was due to insufficient epoxy resin bond strength at the rib and face interface. For our configuration, the epoxy could not provide

* Corresponding authors.
E-mail addresses: jfhunt@fs.fed.us (J.F. Hunt), zcai@fs.fed.us (Z. Cai).

http://dx.doi.org/10.1016/j.compositesa.2015.12.017
1359-835X/

enough capacity to resist core:face interface shear failure. One method to strengthen the interface and avoid premature debonding failure was to develop a slot and tab (S/T) construction technique at the core:face interface. The purpose of slot and tab construction technique was to improve the load transfer between the core and faces utilizing both increased surface area and mechanical interlock load transfer. In this paper, the S/T construction was used to compare the static bending and fatigue bending behavior for the tri-axial core wood-based structural panels.

2. Materials properties

The main material used for both the core and face components to then fabricate the panels was NP610 phenolic impregnated laminated paper obtained from Norplex-Micarta Inc. (Postville, Iowa, USA). Its mechanical properties were obtained using in-house ASTM D638-10 [20] and D695-10 [21] standard coupon tests. Epoxy resin was used to bond the laminated paper faces and core components of the panels. It was obtained from U.S. Composites (West Palm Beach, Florida, USA). The ratio of epoxy to hardener was 3:1. The shear strength for the epoxy was determined using the lap shear test, ASTM D5868-01 [22]. The average epoxy shear strength between the laminated papers was 17.9 MPa, which was significantly less than the laminated paper composite's shear strength of 84.1 MPa. The material properties of the individual components used in the structural panels are listed in Table 1.

3. Design and construction

3.1. Configuration of wood-fiber-based structural panels

The structural composite panels were fabricated by the tri-axial core configuration using the laminate paper as linear ribs in each of three axes with an interlocked structure (Fig. 1). The core rib height was 33.0 mm. The slots in the linear ribs were cut slightly oversized to accommodate the 60° angular orientation between the ribs when assembled. For this study, the slot spacing for all pieces was 117.3 mm, thus creating an equilateral triangle. The thickness of the ribs was 2.4 mm. Two layer laminated paper sheets were used for the faces with or without slot configuration. The combined thickness for both face components used in this study was 5.2 mm including the glue interface. Three centrally located ribs were used to fabricate the core. Cross ribs were cut flush with the width of the panel.

3.2. Slot and tab (S/T) construction technique

For our configuration, the core:face interface was basically only the width or the thickness of the laminated paper ribs, 2.4 mm, times the length of each rib. Due to the relatively small shear interface area and low bonding strength of the epoxy, a new fastening construction technique of S/T was developed to increase the mechanical and interaction epoxy bond area between the ribs and faces. The combined mechanical and adhesive interaction was intended to provide improved interfacial stress transfer to enhance panel strength and avoid premature interface failure. The core components were all machined without or with tabs that were 19.1 mm long spaced every 38.1 mm apart on both sides of the rib. The height of the tabs was 2.3 mm and slightly less than the thickness of the laminate paper (2.4 mm). On the first face layer on either side of the ribs, slots were machined with one-third of the slots arranged along the length of the panel, a second one-third of the slots were aligned 60 degrees off-axis from the first, and a third one-third of the slots were aligned −60 degrees off-axis from the first slots. The slot pattern was made with round

Table 1
Material properties for the panel components.

Materials	Density (kg/m^3)	Comp. strength MD[a] (MPa)	Comp. strength CD[b] (MPa)	Tensile strength MD[a] (MPa)	Tensile strength CD[b] (MPa)	In-plane shear strength (MPa)	MOE MD[a] (GPa)	MOE CD[b] (GPa)	In-plane shear modulus (GPa)	Poisson ratio MD[a]	Poisson ratio CD[b]
Laminated paper (LP)	1387	195.1	168.7	173.9	118.6	84.1	11.6	8.3	3.4	0.36	0.22
Epoxy resin	1101	105.9	–	31.0	–	17.9	1.4	–	–	0.42	–

[a] MD: machine direction.
[b] CD: cross-machine direction.

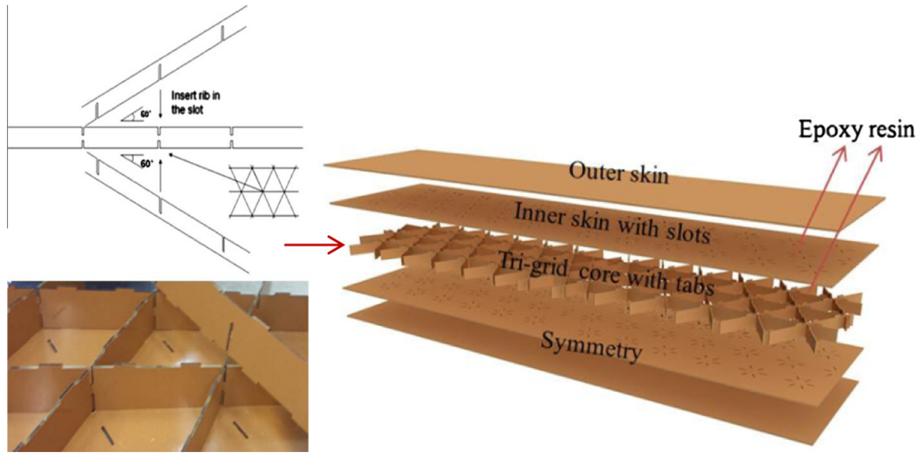

Fig. 1. Panel configuration with tri-axial rib slot orientation and slot and tab construction technique between the ribs and faces. (For interpretation of the references to color in this figure legend, the reader is referred to the web version of this article.)

ends and straight sides just slightly wider than the laminate thickness, 2.4 mm, and slightly longer than the tabs, 20.3 mm in length. The slots were centrally located over the tabs. After the ribs were interlocked into the tri-axial core, the tabs were inserted into the slots on the top and bottom faces. Epoxy had been pre-applied to the inside surface and into the slots prior to inserting the tabs into the slots. The second or top layer of the laminated paper faces were bonded on the top of the slotted faces, Fig. 1. Each triangular repeatable element had 6 pairs of tab and slot in both top and bottom core:face interfaces. All the ribs and slots were cut using a numerically controlled machine for precise alignment. Before applying epoxy resin to any surface it was first prepared by slightly sanding the glue side, and then 404 g/m^2 epoxy resin was spread on each core:face interface for fabrication. A spread rate of 269 g/m^2 of epoxy resin was used to bond the inner and outer faces. The same procedure was used for the panels without S/T construction technique that were used as the control group in this study. Three panel replicates for each stress level were fabricated and tested for the reasonable repeatability.

4. Testing approaches

4.1. Static bending testing

Four point bending test, ASTM C393 [23], was used to investigate the static bending behavior and the results used as reference for load control for the fatigue tests. Six panels were fabricated and statically tested to failure; three panels without S/T configuration were used to compare with the other three panels with the S/T configuration. The span of the simply supported panel was 914 mm (Fig. 2(a)). The width of the panel was 267 mm. A 25 mm LVDT (Linear Variable Differential Transformer) was used to measure the bending deflection (±0.02 mm) at the bottom of the mid-span section. A 45 kN (±0.25%) Instron 5587 Test Machine was used for this static bending test with 5 mm/min head speed. The static bending test set-up is shown in Fig. 2(b).

Based on ASTM C393, the face stress in bending can be calculated by:

$$\sigma_{face} = \frac{Pl}{3t(d+c)b} \tag{1}$$

where P is the applied load, d is the sandwich total thickness, c is the core thickness, t is the facing thickness, l is the span and b is the panel width. The shear stress for solid core can be calculated by equation from ASTM C393-06 [23]. However, this equation was inadequate to estimate the equivalent shear stress of linear rib in the tri-axial structural core. Therefore, the equation was modified to estimate the shear stress of linear rib in the core as equivalent I-beam structures based on the equivalent shear stiffness.

$$\tau_{rib} = \frac{A_s}{A_I}\frac{P}{(d+c)b} \tag{2}$$

where A_s is cross-sectional area of equivalent solid core based on ASTM C393-06, and A_I is the cross-sectional area of equivalent I-beam of tri-axial structural core [12].

The bending stiffness can be determined from Eq. (4),

$$K = \frac{slope \cdot a}{48}(3l^2 - 4a^2) \tag{3}$$

where the *slope* = $P/\triangle$ between 20% and 40% max load, $\triangle$ is the deflection, l and a represent the bending span and the distance from the support to the load point, respectively.

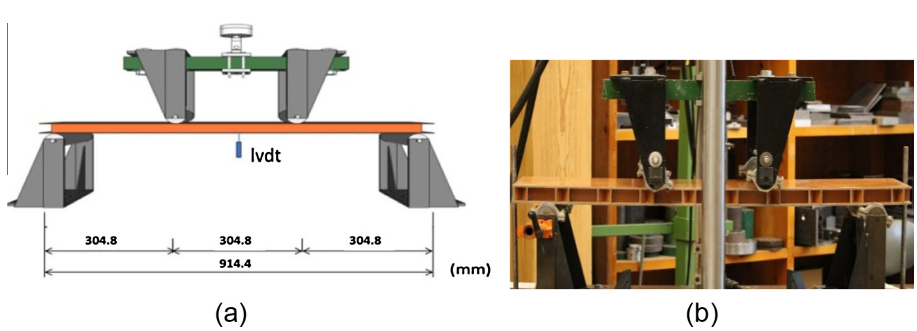

Fig. 2. Static bending test set-up: (a) bending test dimensions; and (b) panel during a static bending test. (For interpretation of the references to color in this figure legend, the reader is referred to the web version of this article.)

4.2. Fatigue testing

This was our first attempt to investigate fatigue performance of the sandwich construction panels. Since all the panels were fabricated from laminated paper composite material, the characteristics of the laminated paper were more like a stiff plastic than MDF or fiberboard. They were consistent in their mechanical properties with a coefficient of variation less than 5%. After consulting with a statistician, we constructed three panels for each stress level based on ASTM D7774 [24], and we believed that the results were representative for the other panels tested at the same stress level. Twenty-four panels were fabricated for the fatigue bending tests. There were four stress levels of panels with and without S/T construction, respectively. The panel design and testing set-up for the fatigue tests were the same as the panels in the static bending test. A MTS 204.12 servo-hydraulic actuator with a compression/tension capacity of ±17.8 kN were set up in the laboratory at room temperature for the fatigue tests. The ultimate face stress in the static bending test was calculated by Eq. (1), and 40%, 50%, 60% and 70% of ultimate face stress of the panels were used to set the maximum load applied for the fatigue test for the panels with S/T construction. For the panels without the S/T configuration, stress levels were reduced to 30%, 35%, 40%, and 50% of ultimate face stress levels and the subsequent maximum load. The load levels were reduced for the panels without the S/T configuration because preliminary fatigue tests had shown reduced fatigue capacity for panels without the S/T configuration. By lowering the fatigue loads for the panels without S/T configuration it was hoped to provide better data for the S–N (stress to number of cycles) curve that might have more uniformly distributed data. The load-cycle frequency was limited to 1 Hz due to the requirement of common applications and capacity of the hydraulic servo controller for panel deflection of 25 mm. The signal was sinusoidal with constant amplitude load ratio $R = 0.1$. Fatigue test completion was determined either when panel failure occurred or when the panel withstood 1 million cycles. All the panels were tested in the laboratory environment around 65% RH (±3%) and 23 °C (±3 °C).

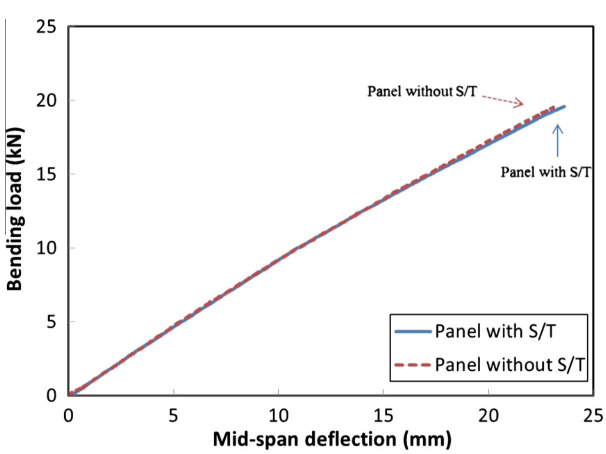

Fig. 3. The typical relationships between static bending load vs. mid-span deflection for panels with and without S/T construction. Each curve represents the mean of three replicates. (For interpretation of the references to color in this figure legend, the reader is referred to the web version of this article.)

5. Results and discussions

5.1. Static bending

Fig. 3 shows the typical relationship between load and mid-span deflection for the panels with and without S/T construction. The results showed that the panels with S/T construction have a similar load/deflection curve compared with the panels without S/T construction. The average failure load for the panels with S/T construction was 19.2 kN at 22.2 mm deflection at the mid-span. Similarly, panels without S/T construction had a maximum load of 20.1 kN at 24.9 mm deflection, Table 2. The estimated maximum face stress of 55.7 MPa for panels with S/T construction and 56.2 MPa for panels without S/T construction were determined from Eq. (1). The core shear stress in the rib of the core was estimated using Eq. (2) were 35.4 and 36.5 MPa, respectively (Table 2).

5.2. Fatigue tests

5.2.1. Fatigue properties

Table 3 shows the average fatigue properties for panels with or without S/T construction. The fatigue test load for each stress level was calculated using the maximum normal stress obtained from static bending tests. The fatigue bending loads for the panels with S/T construction were set at the 40%, 50%, 60%, and 70% of the maximum normal stress, obtained at bending loads of 7.8 kN, 9.8 kN, 11.7 kN, and 13.7 kN, respectively. For the panels without S/T configuration, the following loads of 5.9 kN, 6.9 kN, 7.8 kN, and 9.8 kN, respectively were used for 30%, 35%, 40%, and 50% stress levels. The minimum fatigue loads for each test were calculated using $R = 0.1$.

The results of fatigue life for the panels with S/T construction at the lowest stress level of 40%, the panels had a fatigue life above 1 million cycles. Whereas, the panels without S/T construction required a lower stress level of 30% to reach 1 million cycles. Comparison at the 50% stress level showed panels with S/T construction had 267,120 cycles before failure or 11 times higher than the panels without S/T construction that failed at 23,954 cycles. For both configurations, as the fatigue load level increased, the fatigue life cycles dramatically decreased. The panels with S/T construction had less variation than the panels without S/T construction. The average coefficient of variation for the panels with S/T construction was 14.9% and the panels without S/T construction was 29.1%.

5.2.2. Load–deflection relationship

The typical displacement vs. cycles relationships at each stress level for both types of the panels with and without S/T are shown in Fig. 4(a) and (b), respectively. As expected, the fatigue panels initial deflections exhibited deflections similar to the panels under static bending, Fig. 3. Fig. 4 also shows a good comparison for the panels that withstood the fatigue life of 1 M cycles, those at the

Table 2
Static panel bending properties.

Group	Bending load F_{max} (kN)	Max deflection Δ_{max} (mm)	Face stress σ_{face} (MPa)	Core stress τ_{core} (MPa)	Bending rigidity D (kN m^2)
Panels with S/T	19.2 (10.8)[c]	22.2 (14.1)	55.7 (10.9)	35.4 (11.2)	13.1 (6.1)
Panels without S/T	20.1 (7.8)	24.9 (3.4)	56.2 (8.0)	36.5 (8.0)	12.4 (0.8)

[c] Number in parentheses is coefficients of variation, in percent.

Table 3
Panel fatigue properties as a function of stress level.

Types	Group	Stress level (%)	Maximum fatigue load (kN)	Minimum fatigue load (kN)	Fatigue cycles (N)
Panels with S/T	A	Control	–	–	–
	B	40	7.8	0.78	10^6
	C	50	9.8	0.98	267,120 (24)[c]
	D	60	11.7	1.17	62,057 (17)
	E	70	13.7	1.37	15,025 (18)
Panels without S/T	F	Control	–	–	–
	G	30	5.9	0.59	10^6
	H	35	6.9	0.69	81,676 (34)
	I	40	7.8	0.78	128,315 (9)
	J	50	9.8	0.98	23,954 (74)

[c] Numbers in parentheses are coefficients of variation, in percent.

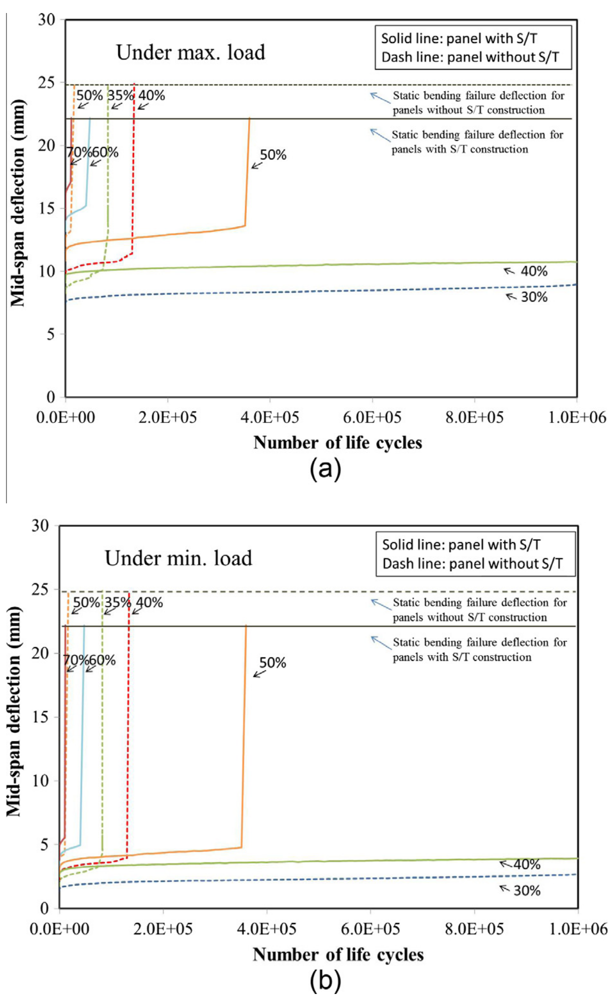

Fig. 4. Typical mid-span panel deflections at each stress level as a function of cycles for both types of panels. (a) Deflection at maximum load; and (b) deflection at minimum load. (For interpretation of the references to color in this figure legend, the reader is referred to the web version of this article.)

40% stress level for the panels with S/T configuration and the panels at the 30% stress level without the S/T configuration. This comparison showed that the relative displacement (RD) (within each cycle) between the maximum fatigue load and minimum fatigue load for the panels with S/T construction only increased 7.5% after 1 M cycles compared with initial (RD) whereas the RD for the panels without S/T configuration was 12.5%. Macro crack propagation at the core:face interface for the panels with S/T configuration seemed to be minimized. The panels with S/T at the 70% stress level had a similar curve as the panels without S/T but at the 50% stress level. For stress levels of 50%, 60%, and 70% of the panels with S/T construction, the deflection rate increased as load levels increased for the panels with S/T construction, as expected. Obviously, the higher stress levels had an increased effect on deflection due to accumulated damage. For the panels without S/T construction, the fatigue cycles at the 35% stress level was less than 40% stress level because of the high variation. The deflection rate quickly increased at the 50% stress level. To reduce the data file size for each test, deflection data was only captured for a decreasing number of cycles as the cycle count increased. Deflection data was collected every 1 cycle from 1 to 100 cycles, every 100 cycles from 100 to 1000, every 1000 cycles from 1000 to 10,000 cycles and 10,000 cycles after that to 1 M. Since the failure did not occur at exactly one of these data collection cycles, the final deflection line was drawn as a straight line vertical line to the static failure deflection point at the last known total cycle number The vertical line is meant as a reference line showing the difference between cyclic failure and static failure loads.

5.2.3. Fatigue damage mechanisms

The typical fatigue failure processes for the panels with or without S/T construction at 50% stress level under the same fatigue bending load were shown in Fig. 5(a) and (b), respectively. The failure processes for the panels with S/T construction showed micro cracks that started to occur at the core:face interfaces only after the first several load cycles, and then the micro cracks continued to propagate along as the cycles increased. For the panels with S/T configuration some of the load was transferred through the tabs. This was observed from the 45 degree major cracks propagating in the ribs from the leading edge of the tab. This major crack propagated through the entire rib up to failure as the cycles increased, as expected. For comparison, the typical fatigue failure for the panels without S/T construction is shown in Fig. 5(b), The panel suddenly failed at the epoxy core:face interface where the shear load over the reduced interface area (due to micro-cracks) reached maximum failure shear stress. There was no shear crack propagation into the rib, thus failure was limited only to the strength of the epoxy resin. The panels with S/T construction at 40% stress level lasted to 1 million cycles having only a few micro cracks in the

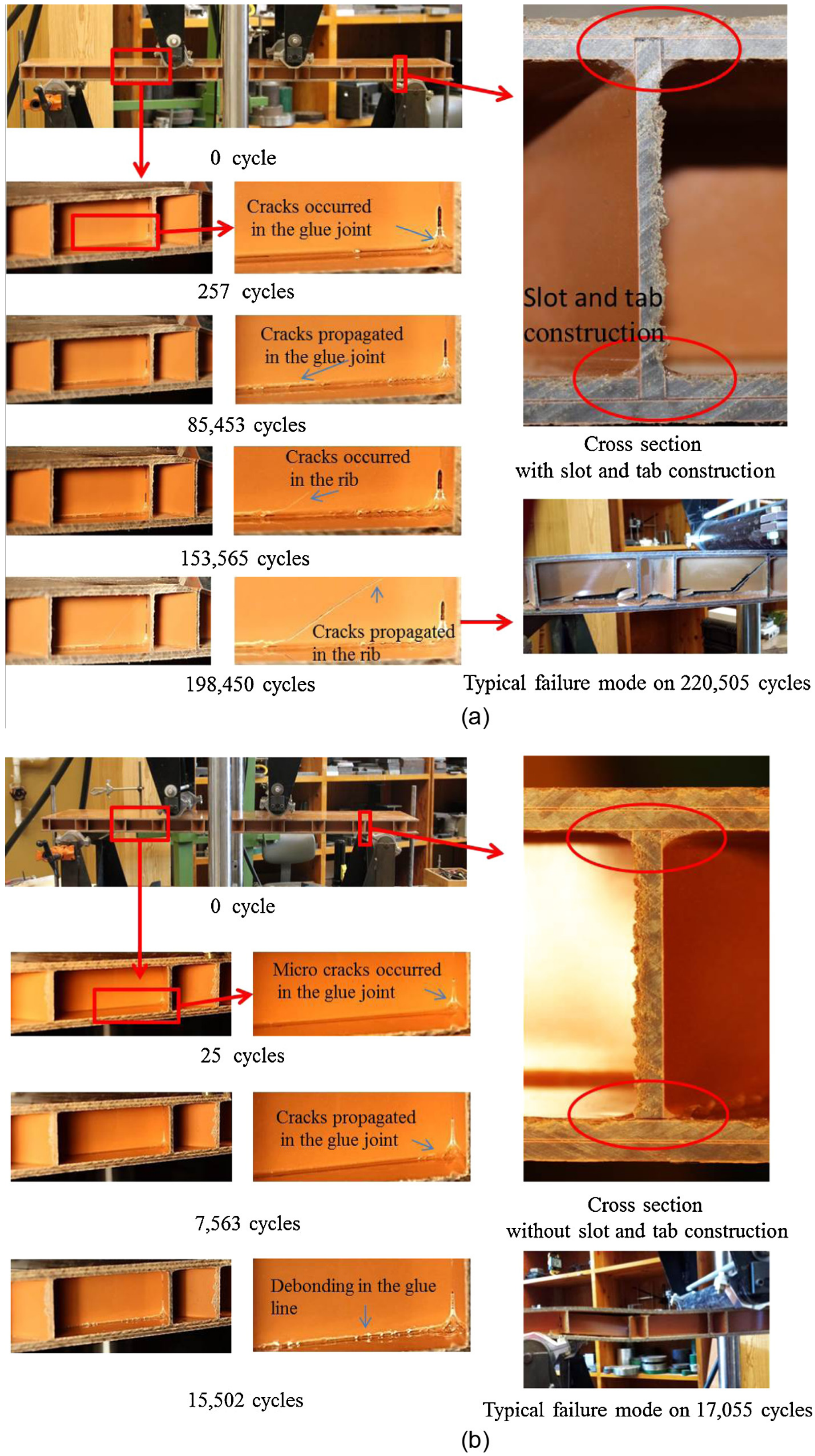

Fig. 5. Typical fatigue failure progression: (a) the panels with S/T construction at 50% stress level; and (b) the panels without S/T construction at 50% stress level. (For interpretation of the references to color in this figure legend, the reader is referred to the web version of this article.)

core:face interfaces, but there was no observed shear crack in the ribs. This indicates that the shear load was transferred into the ribs through the S/T connection whether through mechanical and the increased bonded area.

5.2.4. Fatigue life-stress relationship (N–S curve)

One objective of this study was to determine an approximate model for the relationship between the applied stress and fatigue life (N–S curve) to evaluate the fatigue performance using a possible logarithmic function relationship. A logarithmic regression model, Eq. (4), was fitted to the experimental data.

$$S = A\,In(N) + B \quad (4)$$

where S is the stress level defined as the percentage of applied stress to the predicted static strength and N is the number of cycles-to-failure. A and B are constants related to the materials and configuration.

In Fig. 6, the regression analyses were fit with the experimental data where constants A and **B** were determined. The cycles-N curve for the panels with S/T construction was between 10% and 20% higher than that of the panels without S/T configuration in the range of stress level.

5.2.5. Bending stiffness degradation

The typical bending stiffness degradations for the panels with and without S/T on the same bending load at the 40% stress level are shown in Fig. 7. The panel with S/T construction did not fail within 1 M cycles, while the panel without S/T construction failed after around 134,090 cycles. From Fig. 7, it shows that the initial dynamic bending stiffness of panel with S/T construction was slightly higher than the panel without S/T construction. The panels with S/T at 40% stress level had slower stiffness degradation as cycles increased. This panel had only around 4% loss of bending stiffness during the fatigue life. The S/T structure combined the relative displacement of the core and face with the tab and resin to reduce the total stress at the bonding interface to improve the core:face interface performance. The bending stiffness of the panel without S/T construction had a rapid decrease during the fatigue life, especially near the end of the fatigue life.

The typical bending stiffness degradation for the panels with and without S/T at the same load of 50% stress level are also shown in Fig. 7. Both sets of panels with and without S/T construction failed at this stress level. The panel with S/T construction also had a slightly higher initial dynamic bending stiffness compared with the panel without S/T construction. As the cycles increased, the dynamic bending stiffness for the panel with S/T construction gradually decreased before the interface lost its capacity, then the rib cracks occurred starting at the tab edge. The panel without S/T construction had a sharp degradation during the fatigue life time. It is assumed that the once micro-cracks propagate through the resin, that the shear capacity quickly diminished causing an increased rate of deflection leading to total shear failure.

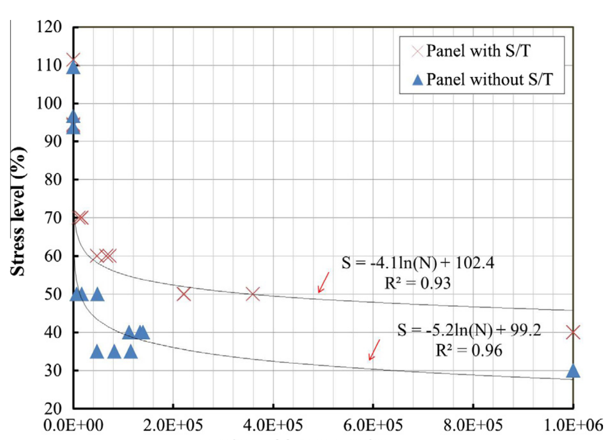

Fig. 6. The relationship between stress level and fatigue life cycle. (For interpretation of the references to color in this figure legend, the reader is referred to the web version of this article.)

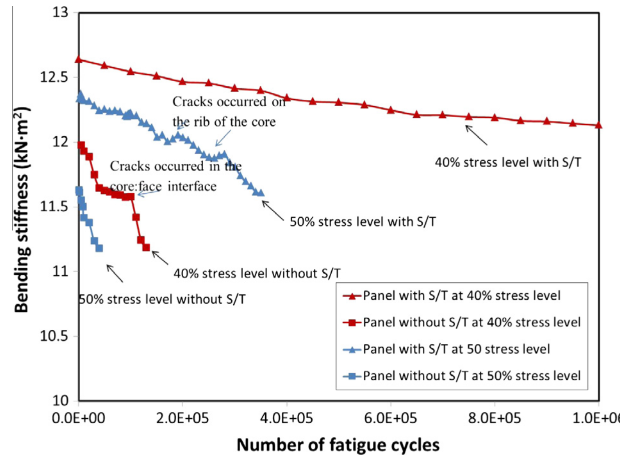

Fig. 7. Typical bending stiffness degradation for panels with S/T and without S/T at the 40% and 50% stress levels. (For interpretation of the references to color in this figure legend, the reader is referred to the web version of this article.)

6. Conclusions

In this work, wood-based structural panels made from phenolic impregnated laminated paper were designed and fabricated with and without S/T configuration. Comparisons were made based on the mechanical performances of the static bending and fatigue tests. Static test results showed there were similar strength, stiffness and failure mode for panels with and without S/T configuration. For the fatigue test results, the results showed that the panels with S/T configuration had more fatigue life cycles than the panels without S/T configuration in the same stress level. At 40% and 50% stress levels, the panels with S/T configuration had less deflection increase than the panels with S/T configuration. The number of micro-cracks and length of the cracks increased in the core:face interfaces for panels with and without S/T configuration as bending load and cycles increased. Although the S/T configuration had little effect on the static bending performance, the S/T construction technique had a significant improvement on fatigue performance due to the combined load sharing capability of the tabs within the slots and the increased core:face epoxy bonded area. The results also showed that the shear load was effectively transferred into the ribs. This transfer caused failure cracks within the ribs, which was not evident in the panels without S/T construction. The panels without S/T construction only had core:face interface debonding failure. A logarithmic curve was fit to the experimental fatigue data to obtain the S–N diagrams for both types of the panels. The S–N curve results indicated the panels with S/T configuration had between 10% and 20% higher stress level at same fatigue cycle than the panels without S/T configuration. A comparison of the bending stiffness degradation similarly showed that the panels with S/T construction had a slower decrease in bending stiffness than panels without S/T construction. It is believed that the S/T configuration could be used to improve fatigue performance for wood-based structural panels.

Acknowledgements

This work is supported by USDA Forest Service, Forest Products Laboratory and the authors gratefully acknowledge the support of Sara Fishwild, James Bridwell, Marshall Begel, Dave Simpson and Marc Joyal of EMRSL group for the mechanical testing.

References

[1] Vasiliev VV, Barynin VA, Rasin AF. Anisogrid lattice structures survey of development and application. Compos Struct 2001;54:361–70.

[2] Wei X, Tran P, De Vaucorbeil A, Ramaswamy RB, Latourte F, Espinosa HD. Three-dimensional numerical modeling of composite panels subjected to underwater blast. J Mecha Phys Solids 2013;61(6):1319–36.

[3] Davalos JF, Qiao PZ, Xu XF, Robinson J, Barth KE. Modeling and characterization of fiber-reinforced plastic honeycomb sandwich panels for highway bridge applications. Compos Struct 2001;52:441–52.

[4] Sharaf T, Fam A. Experimental investigation of large scale cladding sandwich panels under out-of-plane transverse loading for building applications. J Compos Constr 2011;13(3):422–30.

[5] Gibson LJ, Ashby MF. Cellular solids: structure and properties. Cambridge: Cambridge University Press; 1997.

[6] Deshpande VS, Ashby MF, Fleck NA. Foam topology bending versus stretching dominated architectures. Acta Mater 2001;49:1035–40.

[7] Han DY, Tsai SW. Interlocked composite grids design and manufacturing. J Compos Mater 2003;37:287–316.

[8] Fan HL, Meng FH, Yang W. Sandwich panels with kagome lattice cores reinforced by carbon fibers. Compos Struct 2007;81:533–9.

[9] Belingardi P, Martella P, Peroni L. Fatigue analysis of honey-composite sandwich beams. Compos A 2007;38:1183–91.

[10] Jen YM, Ko CW, Lin HB. Effect of the amount of adhesive on the bending fatigue strength of adhesively bonded aluminum honeycomb sandwich beams. Int J Fatigue 2009;31:455–562.

[11] Jen YM, Ko CW, Lin HB. Effect of thickness of face sheet on the bending fatigue strength of adhesively bonded aluminum honeycomb sandwich beams. Eng Fail Anal 2009;16:1282–93.

[12] Li JH, Hunt JF, Cai ZY, Zhou XY. Bending analyses for 3D engineered structural panels made from laminated paper and carbon fabric. Compos B 2013;53:17–24.

[13] Li JH, Hunt JF, Gong SQ, Cai ZY. High strength wood-based sandwich panels reinforced with fiberglass and foam. Bioresources 2014;9(2):1898–913.

[14] Li JH, Hunt JF, Gong SQ, Cai ZY. Testing and evaluation of a slot and tab construction technique for light-weight wood-based structural panels under bending. J Test Eval 2016;44(1):1–10.

[15] Li JH, Hunt JF, Gong SQ, Cai ZY. Simplified analytical model and balanced design approach for light-weight wood-based structural panel in bending. Compos Struct 2016;136:16–24.

[16] Li JH, Hunt JF, Gong SQ, Cai ZY. Fatigue behavior of wood-fiber-based tri-axial engineered sandwich composite panels. Holzforschung 2015. http://dx.doi.org/10.1515/hf-2015-0091.

[17] Li JH, Hunt JF, Gong SQ, Cai ZY. Wood-based tri-axial sandwich composite materials: design, fabrication, testing, modeling and application. In: CAMX conference proceedings. Orlando, FL, 2014. p. 232–47.

[18] Wei L, McDonald AG, Stark NM. Grafting of bacterial polyhydroxybutyrate (PHB) onto cellulose via in situ reactive extrusion with dicumyl peroxide. Biomacromolecules 2015;16:1040–9.

[19] Wei L, Stark NM, McDonald AG. Interfacial improvements in biocomposites based on poly (3-hydroxybutyrate) and poly (3-hydroxybutyrate-co-3-hydroxyvalerate) bioplastics reinforced and grafted with α-cellulose fibers. Green Chem 2015;17:4800–14.

[20] ASTM C638-2010. Standard test method for tensile properties of plastics. ASTM Standards International.

[21] ASTM C695-2010. Standard test method for compressive properties of rigid plastics. ASTM Standards International.

[22] ASTM D5868-01. Standard test method for lap shear adhesion for fiber reinforced plastic (FRP) bonding. ASTM Standards International.

[23] ASTM C393-2006. Standard test method for core shear properties of sandwich constructions by beam. ASTM Standards International.

[24] ASTM Standard D7774-2012, Standard test method for flexural fatigue properties of plastics. ASTM Standards International.